Ising and Bloch domain walls in a two-dimensional parametrically driven Ginzburg-Landau equation model with nonlinearity management

Yu. B. Gaididei
Bogolyubov Institute for Theoretical Physics, Metrologichna Street 14 B, 03680, Kiev, Ukraine

P. L. Christiansen
Department of Informatics and Mathematical Modelling and Department of Physics, Technical University of Denmark, DK-2800 Kongens Lyngby, Denmark

(Received 17 April 2008; published 25 August 2008)

We study a parametrically driven Ginzburg-Landau equation model with nonlinear management. The system is made of laterally coupled long active waveguides placed along a circumference. Stationary solutions of three kinds are found: periodic Ising states and two types of Bloch states, staggered and unstaggered. The stability of these states is investigated analytically and numerically. The nonlinear dynamics of the Bloch states are described by a complex Ginzburg-Landau equation with linear and nonlinear parametric driving. The switching between the staggered and unstaggered Bloch states under the action of direct ac forces is shown.

DOI: 10.1103/PhysRevE.78.026610 PACS number(s): 05.45.Yv, 47.54.−r

I. INTRODUCTION AND MODEL

The parametrically driven Ginzburg-Landau (GL) equation for the complex order parameter $\psi(\vec{r},t)$,

$$\partial_t\psi=(\gamma+i\nu)\psi+(b+ib')\nabla^2\psi-(c+ic')|\psi|^2\psi+\mu\psi^*, \tag{1}$$

is one of the generic equations of condensed matter physics [1]. It describes a large variety of nonlinear physical and chemical systems, such as surface waves in viscous liquids [2,3], parametrically driven chains of coupled nonlinear oscillators [4,5], optical parametric oscillators [6,7], vectorial Kerr-cavity solitons [8], dynamic phase transitions in uniaxial [9,10] and easy plane [11,12] Heisenberg ferromagnets, and light-sensitive Belousov-Zhabotinsky reactions [13,14].

In Eq. (1) $\gamma>0(\gamma<0)$ accounts for linear gain (loss), ν is the detuning parameter, $\nabla=(\partial_x,\partial_y,\partial_z)$ [∂_u stands for $\partial/\partial u$ $(u=x,y,z,t)$]. The parameter $b(b')$ is the diffusion (dispersion) coefficient; the coefficients c and c' characterize nonlinear effects in the system: the saturation effect and nonlinear frequency shift, respectively. The last term in Eq. (1) describes a parametric pump with the forcing amplitude μ.

Recent advances in microstructure technology have made it possible to fabricate various dispersion- and nonlinearity-managed systems where the charge and energy transport can be effectively designed and controlled [15]. Examples are nonlinear photonic band-gap materials, periodic nonlinear superlattices [16], photonic crystals with embedded defect structures such as microcavities, waveguides, and waveguide bends [17,18], optical fibers with periodically sign-alternating group velocity [19], and dispersion management of matter waves by utilizing an optical dipole potential acting as a one-dimensional periodic waveguide [20]. Nonlinearity management was originally proposed as a tool to support the propagation of intense optical beams in layered Kerr media [21–23]. A stabilization of the beam through nonlinearity management in layered Kerr media consisting of glass and air was experimentally demonstrated [24]. Nonlinearity management was also used to avoid collapse in Bose-Einstein condensates [25,26].

Quite recently numerical and experimental investigations of phase-locked multicore fiber lasers showed that by using a special design with two types of active cores one can achieve a generation of spatially flat supermode where all active cores work in phase [27]. Linearly coupled GL equations provide a model for such a type of ring lasers where the active cores are evanescently coupled. Various types of localized states and their stability in dissipative nonlinear media based on linearly coupled GL equations are intensively studied in literature. The main attention was paid to the case of nonparametrically driven two linearly coupled GL equations [28–32] (see also a very comprehensive review paper [33]) where it was shown that by using a dual-core optical fiber with linear gain in an active core and linear loss in the passive (idle) core, one can produce stable pulses in the system. Localized states in a triangular set of linearly coupled cubic-quintic GL equations were considered recently in [34] where stability regions for various types of localized patterns, including stationary and breathing triangular vortices, were found.

In the present work, we consider a parametrically driven cubic GL equation model with nonlinearity management. The medium consists of L alternating waveguides: active and idle ones, with gain and nonlinearity in the active waveguide and loss in the idle waveguides (Fig. 1). The system under consideration is described by the equation

$$\tau_i\partial_t\psi(\vec{r},t)=\ell^2\partial_s^2\psi+\ell_{id}^2\partial_z^2\psi-\gamma_i\psi+[(\ell_a^2-\ell_{id}^2)\partial_z^2\psi-(\tau_a-\tau_i)\partial_t\psi+F(\psi,\psi^*)]\sum_n H_n(s), \tag{2}$$

where

$$H_n(s)=\begin{cases}1 & \text{if } |s-\lambda n|<\dfrac{w}{2},\\ 0 & \text{otherwise}\end{cases}$$

is the structure function, s is the arclength along the circumference, w is the width of the active waveguide (we will also

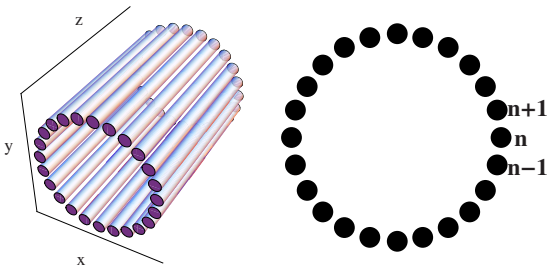

FIG. 1. (Color online) Schematic view of the system with nonlinearity management. The active region is concentrated in cylinders $N=24$, the blank part between cylinders represents the passive (idle) medium.

use the term "window" for the active waveguide) and $\lambda(\lambda \geqslant w)$ is the distance between the centers of the active waveguides. Thus width of the idle region is $\Delta s=\lambda-w$. In Eq. (2) $\tau_i(\tau_a)$ is the relaxation time in the idle (active) region, $\ell_{id}=\sqrt{b_{id}+ib'_{id}}$ ($\ell_a=\sqrt{b_a+ib'_a}$) is the complex longitudinal coherence length in the idle (active) region, $\ell=\sqrt{b+ib'}$ is the complex transversal coherence length which we assume to be the same in the idle and active regions, and the function

$$F(\psi,\psi^*)=(\gamma_a+\gamma_i)\psi+\mu\psi^*-(c+ic')|\psi|^2\psi \tag{3}$$

gives gain, parametric driving, and nonlinear damping in the active region. Note that the nonlinear dynamics which is governed by the one-dimensional (1D) cubic parametrically driven GL equation (2) with spatially independent coefficients [i.e., Eq. (1) with $b'=c'=0, \nabla\equiv\partial_x$] was studied in detail in Refs. [9,11,12,35–41] for domain walls and for 1D and 2D bright solitons in Refs. [42–44]. It was shown that there are two kinds of domain walls, namely, the so-called Ising and Bloch walls. In the domain wall of the first kind only one component (real or imaginary) of the complex amplitude $\psi(x,t)$ is active, while in the domain wall of the second kind both are active. The stability issue of these nonlinear excitations was clarified in Refs. [37,38,42,43]. The aim of this work is to investigate features which acquire the nonlinear excitations in the parametrically driven complex GL equation model with nonlinear management.

The rest of the paper is organized as follows. In Sec. II, we present a pseudodifferential form of the Ginzburg-Landau equation and consider how the nonlocality effects influence the profile and stability of the Ising domain walls. We also give a systematic derivation of the tight-binding approach in which the dynamics is governed by a system of L linearly coupled one-dimensional GL equations. We assume that the active waveguides are placed along a circumference and consider the stationary states of the system. We show that in addition to periodic Ising states there exist *two* types of Bloch states: staggered and unstaggered ones. We present also a linear stability analysis of the periodic Ising states. In Sec. III we compare our analytical results to results obtained directly by numerical simulations. In Sec. IV we discuss weakly nonlinear dynamics of the periodic Bloch states. In Sec. V we consider the switching of the Bloch state chirality under the action of an external ac field. Section VI presents some concluding remarks.

II. THEORETICAL ANALYSIS

A. Pseudodifferential form of the Ginzburg-Landau equation

The solution of Eq. (2) in the space domain of the superlattice requires extensive calculations. However, in the case of very narrow active regions one can significantly simplify the problem because in most of the domain [except at $s \in (n\lambda-\frac{w}{2}, n\lambda+\frac{w}{2})$, $n=0,\pm1,\pm2,\ldots$] the system obeys linear equations. These equations can be solved in the striped idle regions and connected to the solution in the narrow active waveguides. For the sake of simplicity we will neglect the memory effects and assume $\tau_i\to 0$ (these effects are discussed briefly in Appendix A). Elimination of the waves in the linear media described in Appendix A leads to the following equations for the field $\psi(s,z,t)$ at the active waveguides: $\psi_n(z,t)\equiv\psi(\lambda n,z,t)$,

$$\begin{aligned}\tau_a\partial_t\psi_n(z,t) &= \ell_a^2\partial_z^2\psi_n(z,t)+\gamma_a\psi_n(z,t)+\mu\psi_n^*(z,t)\\ &\quad -|\psi_n(z,t)|^2\psi_n(z,t)-\frac{2\ell\hat{\kappa}}{w\tanh(\hat{\kappa}d)}\psi_n(z,t)\\ &\quad +\frac{\ell\hat{\kappa}}{w\sinh(\hat{\kappa}d)}[\psi_{n+1}(z,t)+\psi_{n-1}(z,t)],\\ n&=0,\pm1,\pm2,\ldots,\end{aligned} \tag{4}$$

where $d=(\lambda-w)/\ell$ is the width of the idle region measured in units of the coherence length ℓ, and

$$\hat{\kappa}\equiv\sqrt{-\ell_{id}^2\partial_z^2+\gamma_i} \tag{5}$$

is the pseudodifferential operator defined as

$$\begin{aligned}\overline{\hat{\kappa}\psi}(k,t) &\equiv \frac{1}{2\pi}\int_{-\infty}^{\infty}dze^{-ikz}\sqrt{-\ell_{id}^2\partial_z^2+\gamma_i}\psi(z,t)\\ &=\sqrt{\ell_{id}^2k^2+\gamma_i}\,\bar{\psi}(k,t).\end{aligned} \tag{6}$$

Thus, the dynamics of the system is described by the set of pseudodifferential or, in other words, by nonlocal in time and space equations. The nonlocal character of the active waveguide dynamics is due to the existence of two pathways for the energy transfer: directly along the active waveguide [the first term on the right-hand side of Eq. (4)] and through the idle region [the last two terms on the right-hand side of Eq. (4)].

One of the physically reasonable excitation patterns is the configuration where the complex amplitudes are the same in all active waveguides, i.e.,

$$\psi_n(z,t)=\Psi(z,t). \tag{7}$$

For this excitation pattern the function of the complex amplitude $\Psi(z,t)$ satisfies the equation

$$\tau_a \partial_t \Psi(z,t) = \ell_a^2 \partial_z^2 \Psi(z,t) + \gamma_a \Psi(z,t) + \mu \Psi^*(z,t) - |\Psi(z,t)|^2 \Psi(z,t) - \frac{2\ell}{w} \times \int_{-\infty}^{\infty} \mathcal{G}(z-z')(-\ell_{id}^2 \partial_{z'}^2 + \gamma_i)\Psi(z',t)dz', \tag{8}$$

where the kernel $\mathcal{G}(z)$ has the form

$$\mathcal{G}(z) = \frac{1}{2\pi}\int_{-\infty}^{\infty} dz e^{-ikz} \frac{\tanh(\sqrt{\ell_{id}^2 k^2 + \gamma_i} d/2)}{\sqrt{\ell_{id}^2 k^2 + \gamma_i}} \approx \frac{4\pi}{\ell_{id}} \frac{\exp(-\sqrt{\gamma_i + 1/d^2}|z|/\ell_{id})}{\sqrt{\gamma_i + 1/d^2}}. \tag{9}$$

Equation (8) has the same structure as the complex GL equation with nonlocal coupling derived in [45] as a reduced form of a universal class of reaction -diffusion systems near the Hopf bifurcation point.

When the sign of the complex amplitudes in the active waveguides alternates,

$$\psi_n(z,t) = (-1)^n \Psi(z,t); \tag{10}$$

the complex amplitude $\Psi(z,t)$ satisfies the same equation as Eq. (8), but the expression for the kernel $\mathcal{G}(z)$ has now the form

$$\mathcal{G}(z) = \frac{1}{2\pi}\int_{-\infty}^{\infty} dz e^{-ikz} \frac{\coth(\sqrt{\ell_{id}^2 k^2 + \gamma_i} d/2)}{\sqrt{\ell_{id}^2 k^2 + \gamma_i}} \approx \frac{4\pi}{\ell_{id}} \frac{\exp(-\sqrt{\gamma_i + 1/d^2}|z|/\ell_{id})}{\sqrt{\gamma_i + 1/d^2}}. \tag{11}$$

In this case Eqs. (8) and (11) have the same structure as the nonlocal complex Ginzburg-Landau equation derived for electrochemical systems with migration coupling [46].

In this paper we assume that $b'=b'_a=b'_{id}=c'=0$, $c=1$ which means that all coherence lengths ℓ, ℓ_a, and ℓ_{id} are real and we rescaled the complex amplitude ψ such that the coefficient in front of the nonlinear term is equal to unity. The set of equations (4) is still very complicated. Therefore we consider two more simple excitation distribution patterns: (i) a spatially uniform excitation distribution along the circumference and (ii) a spatially uniform distribution along the longitudinal coordinate.

B. Ising domain walls in a system with long-range dispersion

In this section we consider how the nonlocality effects influence the profile and stability of the Ising domain walls. We will consider a spatially uniform along the circumference excitation pattern [see Eq. (7)] and neglect the memory effects ($\tau_i=0$). For the sake of simplicity we assume that the excitation energy propagates mainly in the idle region ($\ell_a=0$) and that the excitations have an infinite lifetime in it ($\gamma_i=0$). Considering the systems with small distances between active waveguides $d<1$, one can use a Padé approximation of degree (2,2) [47] for the operator $\hat{\kappa}\tanh(\hat{\kappa}d/2)$ with respect to the variable $\hat{\kappa}d$ and obtain instead of Eq. (8)

$$\tau_i \partial_t X = \ell_i^2 \frac{\partial_z^2}{1 - r^2 \ell_i^2 \partial_z^2} X + (\gamma_a + \mu)X - (X^2 + Y^2)X,$$

$$\tau_i \partial_t Y = \ell_i^2 \frac{\partial_z^2}{1 - r^2 \ell_i^2 \partial_z^2} Y + (\gamma_a - \mu)Y - (X^2 + Y^2)Y, \tag{12}$$

where

$$X(z,t) = \mathrm{Re}\ \Psi(z,t), \quad Y(z,t) = \mathrm{Im}\ \Psi(z,t), \tag{13}$$

and the parameter $r=w/(12\ell d)$ controls the nonlocal effects in the system. The quantity $r\ell_i$ is the radius of the long-range dispersion interaction. When $r\to 0$ the nonlocal effects are unimportant and the pseudodifferential equation (12) takes a conventional differential form (1).

1. Stationary solutions of the nonlocal Ginzburg-Landau equation

It is well known [35] that in the local case ($r=0$) there exist two types of stationary ($\partial_t=0$) spatially inhomogeneous solutions of Eqs. (12): the Ising domain walls

$$X = \pm\sqrt{\gamma_a + \mu}\tanh\left(\sqrt{\frac{\gamma_a + \mu}{2}}\frac{z}{\ell_i}\right), \quad Y = 0 \tag{14}$$

and the Bloch domain walls

$$X = \pm\sqrt{\gamma_a + \mu}\tanh\left(\sqrt{2\mu}\frac{z}{\ell_i}\right), \tag{15}$$

$$Y = \pm\sqrt{\gamma_a - 3\mu}\,\mathrm{sech}\left(\sqrt{2\mu}\frac{z}{\ell_i}\right).$$

In the general case of nonlocal dispersion ($r\neq 0$) the static Ising domain walls are described by the equation

$$\ell_i^2 \frac{\partial_z^2}{1 - r^2 \ell_i^2 \partial_z^2} X + (\gamma_a + \mu)X - X^3 = 0. \tag{16}$$

Acting on Eq. (16) by the operator $1-r^2\ell_i^2\partial_z^2$, we obtain the equation

$$\ell_i^2 \partial_z^2 \{(1 - r^2(\gamma_a + \mu) + 3r^2X^2)\partial_z X\} + (\gamma_a + \mu)X - X^3 = 0, \tag{17}$$

which under the boundary conditions $X\to\pm\sqrt{\gamma_a+\mu}$ ($z\to\pm\infty$) has the solution

$$\sqrt{1 + 2(\gamma_a + \mu)r^2}\,\mathrm{arctanh}\left(\sqrt{1 + 2(\gamma_a + \mu)r^2}\frac{X}{\sqrt{\gamma_a + \mu + 2r^2X^2}}\right) - \frac{3r\sqrt{\gamma_a + \mu}}{\sqrt{2}}\,\mathrm{arcsinh}(\sqrt{2}rX) = \frac{z}{\ell_i}\sqrt{\frac{\gamma_a + \mu}{2}}. \tag{18}$$

Looking at Eq. (18) one can see that near the center of the domain wall where X is small, $\partial_z X \sim (1-\sigma)^{-1/2}$ where the notation $\sigma=(\gamma_a+\mu)r^2$ is introduced. It means that the slope of the domain wall becomes vertical for $\sigma=1$ (see Fig. 2). If

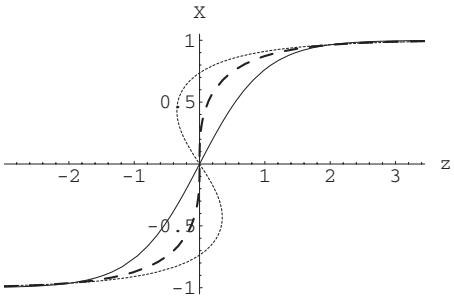

FIG. 2. The Ising domain wall profile for different values of the radius of the nonlocal dispersion: the subcritical case $r\sqrt{\gamma_a+\mu}=0.1$ (solid line), the critical case $r\sqrt{\gamma_a+\mu}=1$ (dashed line), and the supercritical case $r\sqrt{\gamma_a+\mu}=1.5$ (dotted line).

$\sigma>1$ the slope of the domain wall assumes negative values and the solution (18) becomes *S*-shaped (multivalued). A similar situation was observed in Ref. [48] for the case of kinks in the sine-Gordon model with Kac-Baker long-range interactions. It was shown in Ref. [48] that at $\sigma\to 1$ the frequency of an internal shape mode of the kink goes to zero and the kink loses its stability.

2. Linear stability of the Ising domain walls in the nonlocal Ginzburg-Landau equation model

The Ising walls (14) become unstable when $\gamma_a \geqslant \gamma_{cr} \equiv 3\mu$ [9,36] and they bifurcate into Bloch walls. It is of interest therefore to clarify how the nonlocality of the equation influences the Ising-Bloch transition.

To investigate the stability of the Ising state (18) to small perturbations we use the rescaled variables

$$\Psi(z,t) \equiv X(z,t) + iY(z,t) = \sqrt{\gamma_a+\mu}[\mathcal{X} + u(\tilde{z},\tilde{t}) + iv(\tilde{z},\tilde{t})],$$

$$\mathcal{X} = \frac{X}{\sqrt{\gamma_a+\mu}}, \quad \tilde{t} = (\gamma_a+\mu)\frac{t}{\tau_i}, \quad \tilde{z} = \sqrt{\frac{\gamma_a+\mu}{2}}\frac{z}{\ell_i}, \tag{19}$$

where the function $X(z)$ is given by Eq. (18) and assuming that the linear perturbation depends exponentially on time,

$$u(\tilde{z},\tilde{t}) = U(\tilde{z})e^{\Lambda\tilde{t}}, \quad v(\tilde{z},\tilde{t}) = V(\tilde{z})e^{\Lambda\tilde{t}}, \tag{20}$$

we arrive at an eigenvalue problem

$$\partial_{\tilde{z}}^2\{[1+\sigma(\Lambda-1+3\mathcal{X}^2)]U\} - 6\mathcal{X}^2U = 2(\Lambda-1)U, \tag{21}$$

$$\partial_{\tilde{z}}^2\{[1+\sigma(\Lambda-q+\mathcal{X}^2)]V\} - 2\mathcal{X}^2V = 2(\Lambda-q)V, \tag{22}$$

where $q=(\gamma_a-\mu)/(\gamma_a+\mu)$. The Ising state is stable provided that the set of Eqs. (21) and (22), has no positive eigenvalue. For systems with short-range dispersion ($r\to 0$) Eqs. (21) and (22), reduce to

$$\partial_\xi^2 U - 6\tanh^2\xi U = 2(\Lambda-1)U, \tag{23}$$

$$\partial_\xi^2 V - 2\tanh^2\xi V = 2(\Lambda-q)V. \tag{24}$$

Their analysis showed [37] that besides the neutral mode $U=\mathrm{sech}^2\,\xi$, $V=0$ with $\Lambda=0$, which is due to the translational symmetry of the system, there exists a mode $U=0$, $V=\mathrm{sech}\,\xi$ with $\Lambda_0=(\gamma_a-3\mu)/(\gamma_a+\mu)$ which governs the Ising-Bloch transition. The Ising-Bloch transition in such systems occurs when $\gamma_a \geqslant 3\mu$.

The nonlocal model under consideration is translational invariant and therefore the set of Eqs. (21) and (22), also has the neutral mode $U=\partial_{\tilde{z}}\mathcal{X}$, $V=0$ with $\Lambda=0$. However it was impossible to find the exact eigenfunction and the eigenvalue for Eq. (22) which governs the Ising-Bloch transition in the nonlocal case. Let us consider this problem perturbatively. Taking into account that the function $\mathcal{X}$ is given by Eq. (18) in an implicit form it is convenient to change the independent variable from $\tilde{z}$ to $\mathcal{X}$ and as a result instead of Eq. (22) we obtain for the function

$$\mathcal{W}(\mathcal{X}) = \frac{1+\sigma(\Lambda+\mathcal{X}^2-q)}{\sqrt{C(\mathcal{X})}}V, \tag{25}$$

where

$$C(\mathcal{X}) = \frac{1-\sigma(1-3\mathcal{X}^2)}{(1-\mathcal{X}^2)\sqrt{1+2\sigma\mathcal{X}^2}}, \tag{26}$$

an equation in the form

$$\frac{d^2}{d\mathcal{X}^2}\mathcal{W} + \mathcal{U}(\mathcal{X})\mathcal{W} = 0, \tag{27}$$

where

$$\mathcal{U}(\mathcal{X}) = 2\frac{q-\Lambda-\mathcal{X}^2}{1+\sigma(\Lambda+\mathcal{X}^2-q)}C(\mathcal{X}) - \frac{1}{4}\sqrt{C(\mathcal{X})}\frac{d^2}{d\mathcal{X}^2}\left(\frac{1}{\sqrt{C(\mathcal{X})}}\right). \tag{28}$$

In the local limit when $\sigma=0$, Eq. (27) reduces to

$$\frac{d^2}{d\mathcal{X}^2}\mathcal{W} + \mathcal{U}_0\mathcal{W} = 0,$$

$$\mathcal{U}_0 = \frac{1+2(q-\Lambda-\mathcal{X}^2)}{(1-\mathcal{X}^2)^2}. \tag{29}$$

It is straightforward to see that Eq. (29) has the eigenvalue Λ_0 with the eigenfunction

$$\mathcal{W}_0 = 1-\mathcal{X}^2, \tag{30}$$

which corresponds to $\mathrm{sech}(\tilde{z})$ in terms of the original spatial variable. Considering the difference $\mathcal{U}-\mathcal{U}_0$ as a perturbation, we obtain that in the first order perturbation theory the eigenvalue is

$$\Lambda = q - \frac{1}{2} - \frac{19}{30}\sigma + \mathcal{O}(\sigma^2). \tag{31}$$

Thus in the weakly nonlocal Ginzburg-Landau equation model the Ising wall loses its stability for

$$\gamma_a > \gamma_{cr} \equiv 3\mu(1+6.7\mu r^2).$$

This inequality shows that in the nonlocal case the threshold value of the gain γ_{cr} increases as the radius of the long-range interaction r increases.

C. Periodic Ising and Bloch domain wall states

We will consider the system with a strong damping in the idle area, $\gamma_i \gg 1$. In this case one can neglect both the memory effects and effects of long-range coupling. Formally it means that the derivatives in the operator $\hat{\kappa}$ may be omitted and instead of Eqs. (4) we obtain the simpler set of equations

$$\tau_a \partial_t \psi_n(z,t) = \ell_a^2 \partial_z^2 \psi_n(z,t) + \gamma \psi_n(z,t) + \mu \psi_n^*(z,t) - |\psi_n(z,t)|^2 \psi_n(z,t) + J[\psi_{n+1}(z,t) + \psi_{n-1}(z,t) - 2\psi_n(z,t)],$$

$$n = 0, \pm 1, \pm 2, \ldots, \tag{32}$$

which may by called a discrete-continuum GL equation. Here

$$J = \frac{\ell \sqrt{\gamma_i}}{w \sinh(\sqrt{\gamma_i} d)}$$

gives an effective coupling between fibers and the parameter

$$\gamma = \gamma_a - \frac{\ell \sqrt{\gamma_i}}{w} \tanh\left(\frac{\sqrt{\gamma_i} d}{2}\right)$$

gives an effective gain coefficient in the active area. The strong damping of excitations inside the idle region decreases the gain rate and can even completely kill the gain effects. In what follows we will assume that the renormalized gain rate γ is positive. Finally, we consider a necklace-shaped fiber set, consisting of L active cores placed along a circumference (see Fig. 1). In other words, we will consider the Ginzbirg-Landau equation model (32) on a cylinder,

$$\psi_n(z,t) = \psi_{n+L}(z,t), \quad n = 1 \ldots L, \quad -\infty < z < \infty. \tag{33}$$

Equations (32) and (33) can be presented in a gradient form,

$$\tau_a \partial_t \psi_n = -\frac{\delta \mathcal{F}}{\delta \psi_n^*}, \tag{34}$$

or equivalently,

$$\tau_a \partial_t X_n = -\frac{\delta \mathcal{F}}{\delta X_n}, \quad \tau_a \partial_t Y_n = -\frac{\delta \mathcal{F}}{\delta Y_n}, \tag{35}$$

where $X_n = \mathrm{Re}\ \psi_n$, $Y_n = \mathrm{Im}\ \psi_n$, and the energy functional $\mathcal{F}$ is given by the expression

$$\mathcal{F} = \frac{1}{2} \int_{-\infty}^{\infty} dz \sum_{n=1}^{L} \left[\ell_a^2 (\partial_z X_n)^2 + \ell_a^2 (\partial_z Y_n)^2 + J(X_{n+1} - X_n)^2 + J(Y_{n+1} - Y_n)^2 - (\gamma + \mu) X_n^2 - (\gamma - \mu) Y_n^2 + \frac{1}{2}(X_n^2 + Y_n^2)^2 \right] dx. \tag{36}$$

In the case when the characteristic size of excitation is much larger then the lattice spacing one can replace $\psi_n(z,t)$ by the function $\psi(s,z,t)$ of the arclength s, which is the continuum analog of n. Using the Euler-McLaurin formula [49] from Eq. (36) we obtain

$$\mathcal{F} = \frac{1}{2} \int_{-\infty}^{\infty} dz \int_0^L ds \left[\ell_a^2 (\partial_z X)^2 + \ell_a^2 (\partial_z Y)^2 + J(\partial_s X)^2 + J(\partial_s Y)^2 - (\gamma + \mu) X^2 - (\gamma - \mu) Y^2 + \frac{1}{2}(X^2 + Y^2)^2 \right]. \tag{37}$$

In the continuum approach the dynamic of the system is governed by the equations

$$\tau_a \partial_t X = \ell_a^2 \partial_z^2 X + J \partial_s^2 X - (X^2 + Y^2) X + (\gamma + \mu) X,$$

$$\tau_a \partial_t Y = \ell_a^2 \partial_z^2 Y + J \partial_s^2 Y - (X^2 + Y^2) Y + (\gamma - \mu) Y, \tag{38}$$

which we will solve under the boundary conditions

$$X(s + L, z, t) = X(s, z, t), \quad Y(s + L, z, t) = Y(s, z, t),$$

$$\partial_z X|_{z \to \pm\infty} = 0, \quad \partial_z Y|_{z \to \pm\infty} = 0. \tag{39}$$

1. Stationary states

The spatially uniform in the longitudinal z-direction stationary solutions of Eqs. (38) satisfy

$$J \partial_s^2 X - (X^2 + Y^2) X + (\gamma + \mu) X = 0,$$

$$J \partial_s^2 Y - (X^2 + Y^2) Y + (\gamma - \mu) Y = 0. \tag{40}$$

Let us consider now the above parametric GL equation (40) under the periodic boundary conditions (39). It is a straightforward task to find that there are three types of nontrivial stationary spatially imhomogeneous solutions:

(i) *Periodic Ising states*.

$$X_I(s) = \sqrt{\frac{2m}{1+m}(\gamma + \mu)}\, \mathrm{sn}\left(\sqrt{\frac{\gamma + \mu}{(1+m)J}} s \right), \quad Y = 0, \tag{41}$$

here (and in what follows) $pq(x) \equiv pq(x|m)$ $(p,q = \mathrm{c}, \mathrm{s}, \mathrm{d}, \mathrm{n})$ is a Jacobian elliptic function with modulus m [49]. From the boundary condition (39) we find that the modulus m is determined by the equation

$$\gamma + \mu = (1+m) J \frac{16 \mathbf{K}^2}{L^2} j^2, \tag{42}$$

where $\mathbf{K}$ is the elliptic integral of the first kind [49] and j is an integer. The solution (41) exists for $\gamma + \mu \geq 4\pi^2 J / L^2$. In the limit of infinite domain when $m \to 1$ the solution (41) reduces to the Ising-wall profile (14). The finite domain for the order parameter profile is of the form of $2j$ Ising domain walls (Fig. 3).

(ii) *Periodic Bloch states*. In the case of finite domain there are two kinds of Bloch states: in-phase states and staggered states.

The in-phase states are

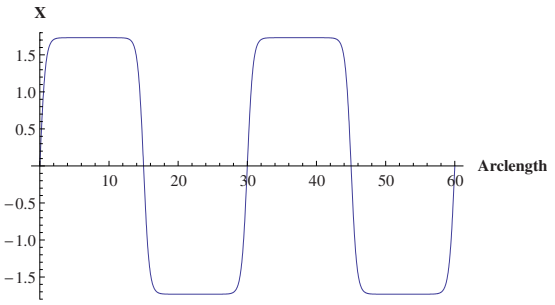

FIG. 3. (Color online) Wall profiles for periodic Ising states ($\gamma=1$, $\mu=1$, $j=2$).

$$X_d = \sqrt{m(\gamma+3\mu-2\mu m)}\,\mathrm{sn}\left(\sqrt{\frac{2\mu}{J}}s\right),$$

$$Y_d = \sqrt{\gamma-\mu-2\mu m}\,\mathrm{dn}\left(\sqrt{\frac{2\mu}{J}}s\right), \tag{43}$$

with the modulus m given by the equation

$$\mu = J\frac{8\mathbf{K}^2}{L^2}j^2. \tag{44}$$

The staggered states are determined by the expression

$$X_c = \sqrt{\gamma+3\mu-\frac{2\mu}{m}}\,\mathrm{sn}\left(\sqrt{\frac{2\mu}{mJ}}s\right),$$

$$Y_c = \sqrt{\gamma-\mu-\frac{2\mu}{m}}\,\mathrm{cn}\left(\sqrt{\frac{2\mu}{mJ}}s\right). \tag{45}$$

Here the modulus m is determined by the equation

$$\mu = J\frac{8m\mathbf{K}^2}{L^2}j^2. \tag{46}$$

Notice that for an infinite system ($L\to\infty$) when $m\to 1$ the solutions (45) and (43) coalesce and reduce to the Bloch domain wall (15). However, for finite domains the solutions (45) and (43) are qualitatively different (see Figs. 4 and 5). This difference can be clearly identified by using a chirality density defined as [50]

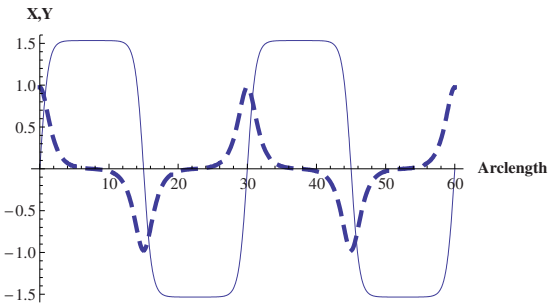

FIG. 4. (Color online) Wall profiles for staggered periodic Bloch states. The real (solid line) and imaginary (dashed line) parts of the complex amplitude are plotted for $\gamma=2$, $\mu=0.35$, $j=2$.

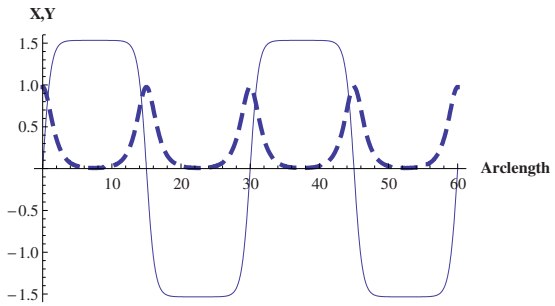

FIG. 5. (Color online) Wall profiles for unstaggered periodic Bloch states. The real (solid line) and imaginary (dashed line) parts of the complex amplitude are plotted for $\gamma=2$, $\mu=0.35$, $j=2$.

$$\chi(s) = Y\partial_s X - X\partial_s Y, \tag{47}$$

and a mean chirality defined as

$$\bar{\chi} = \int_0^L \chi(s)ds. \tag{48}$$

The chirality $\chi=0$ for Ising walls (14) and $\chi\neq 0$ for Bloch walls (15). In the case of finite domains the chirality vanishes for periodic Ising states (41) whereas the chirality density for the staggered and in-phase Bloch periodic solutions is given by the expressions

$$\chi_c = \sqrt{\frac{2\mu}{mJ}\left(\gamma+3\mu-\frac{2\mu}{m}\right)\left(\gamma-\mu-\frac{2\mu}{m}\right)}\,\mathrm{dn}\left(\sqrt{\frac{2\mu}{mJ}}s\right) \tag{49}$$

and

$$\chi_d = \sqrt{\frac{2\mu}{J}}\sqrt{m(\gamma+3\mu-2\mu m)(\gamma-\mu-2\mu m)}\,\mathrm{cn}\left(\sqrt{\frac{2\mu}{J}}s\right), \tag{50}$$

respectively. Thus, both type of Bloch solutions have nonvanishing chirality densities. However, for the in-phase Bloch states the chirality density χ_d is an alternating-sign function while the chirality density χ_c for the staggered Bloch states does not change sign. Consequently the mean chirality $\bar{\chi}=0$ for in-phase Bloch states and $\bar{\chi}\neq 0$ for staggered Bloch states.

2. Linear stability of the Ising periodic states

To study the dynamics of the periodic Ising and Bloch states we use an approach similar to the approach which was developed in [37,38,42,43] for the case of infinite size systems. It is convenient to use the scaled variables

$$\xi = s\sqrt{\frac{\gamma+\mu}{(1+m)J}}, \quad \zeta = \frac{z}{\ell_a}\sqrt{\frac{\gamma+\mu}{1+m}}, \quad \tau = t\frac{\gamma+\mu}{1+m} \tag{51}$$

and present the solution of Eq. (1) in the form

$$\psi = \sqrt{\frac{2m(\gamma+\mu)}{1+m}}[\mathrm{sn}\,\xi + u(\xi,\zeta,\tau) + iv(\xi,\zeta,\tau)]. \quad (52)$$

The real functions $u(\xi,\zeta,\tau)$ and $v(\xi,\zeta,\tau)$ satisfy the equations

$$(\partial_\tau - \partial_\zeta^2)\vec{q} = -\hat{\mathcal{H}}\vec{q} + \vec{N}, \quad (53)$$

where $\vec{q}=(u,v)^T$,

$$\hat{\mathcal{H}} = \begin{pmatrix} \hat{H}_2 - 1 - m & 0 \\ 0 & \hat{H}_1 - \kappa \end{pmatrix}, \quad (54)$$

where the operator $\hat{H}_l(l=1,2)$ has the form

$$\hat{H}_l = -\partial_\xi^2 + l(l+1)m\,\mathrm{sn}^2\,\xi, \quad (55)$$

the vector $\vec{N}=(N_u,N_v)^T$ with

$$N_u = -2m[(3u^2+v^2)\mathrm{sn}\,\xi + uv^2 + u^3],$$

$$N_v = -2m(2uv\ \mathrm{sn}\,\xi + u^2v + v^3) \quad (56)$$

represents the nonlinear terms of the Ginzburg-Landau equation, and the notation $\kappa=(1+m)(\gamma-\mu)/(\gamma+\mu)$ is used.

To investigate the stability of the Ising state (41) to small perturbations we linearize Eqs. (53) (i.e., we neglect the nonlinear terms N_u and N_v) and assuming that the linear perturbation depends exponentially on time and the longitudinal variable ζ,

$$\vec{q}(\xi,\zeta,\tau) = \vec{Q}(\xi)e^{\Omega\tau+ip\zeta},$$

$$\vec{Q}(\xi) = (U(\xi),V(\xi)), \quad (57)$$

we arrive at an eigenvalue problem

$$-\hat{\mathcal{H}}\vec{Q} = \Lambda\vec{Q}, \quad (58)$$

where $\Lambda=\Omega+p^2$. The eigenvalue problem (58) splits in two separate one-dimensional Schrödinger equations with a potential $\mathcal{U}(\xi)=l(l+1)m\,\mathrm{sn}^2(\xi)$. They are the Lamé equations [51].

For an infinite size system ($L\to\infty$) when $m\to 1$ Eqs. (58) reduce to Eqs. (23) and (24). For periodic systems (i.e., for general values of m) Eqs. (58) and (55) describe a quantum particle in the potential $\mathcal{U}(\xi)$ with a period $2\mathbf{K}$. The eigenfunctions $\phi_{j,k}$ and eigenenergies $E_j(k)$ for the Hamiltonian (55) are determined by the equation

$$-\partial_\xi^2\phi + \lambda(\lambda+1)m\,\mathrm{sn}^2(\xi)\phi = E\phi. \quad (59)$$

The eigenfunctions are the Bloch wave functions $\phi_{j,k}^{(l)}(\xi) = e^{ik\xi}\Phi_{j,k}^{(l)}(\xi)$ where $\Phi_{j,k}^{(l)}(\xi)$ has the periodicity of the potential; k is the wave number (momentum) and $j(j=0,1,\lambda\ldots)$ denotes the energy band. The eigenenergies lie within $\lambda+1$ allowed bands separated by λ gaps. There are $2\lambda+1$ eigenfunctions associated to the boundaries of the allowed energy bands: the so-called edge states. For $\lambda=1$ there are two energy bands given by

$$E_0 \leqslant E \leqslant \tilde{E}_0, \quad E \geqslant E_1, \quad (60)$$

with the edge energies given by $E_0=m$, $\tilde{E}_0=1$, $E_1=1+m$. The corresponding edge states, i.e., the states from the set $\phi_{j,k}^{(1)}(\xi)$ with the wave number k at the edges of the Brillouin zone ($k=0$ and $k=\pi/2\mathbf{K}$) are [52,53]

$$\phi_0^{(1)} = \mathrm{dn}\,\xi, \quad \tilde{\phi}_0^{(1)} = \mathrm{cn}\,\xi, \quad \phi_1 = \mathrm{sn}\,\xi. \quad (61)$$

For $\lambda=2$ there are three energy bands

$$E_0 \leqslant E \leqslant \tilde{E}_0, \quad E_1 \leqslant E \leqslant \tilde{E}_1, \quad E \geqslant E_2, \quad (62)$$

with

$$E_0 = 2f_-(m), \quad \tilde{E}_0 = 1+m, \quad E_1 = 1+4m, \quad \tilde{E}_1 = 4+m,$$

$$E_2 = 2f_+(m), \quad (63)$$

where $f_\pm(m)=1+m\pm\sqrt{1-m+m^2}$. The edge states which correspond to the lowest energy band are [52,53]

$$\phi_0^{(2)} = -m\,\mathrm{sn}^2(\xi) + f_+(m)/3, \quad \tilde{\phi}_0^{(2)} = \mathrm{cn}\,\xi\,\mathrm{dn}\,\xi. \quad (64)$$

It follows from Eqs. (59), (62), and (63) that the eigenvalue problem given by Eqs. (58) possesses eigenvectors

$$\vec{Q} = (\phi_{0,k}^{(2)}(\xi),0)^T \quad (65)$$

for which the eigenvalues Λ lie within the interval

$$0 \leqslant \Lambda \leqslant -1-m+2\sqrt{1-m+m^2}. \quad (66)$$

This means that in periodic systems the Ising states are *always* unstable with respect to excitation of the states $\phi_{0,k}^{(2)}(\xi)$. However, from the practical point of view this instability is important only for small size periodic systems. For large enough systems ($L\gg 1$) it is rather weak. Indeed, it follows from Eq. (42) that for $L/j\gg 1$

$$1-m \approx 16\exp\left\{-\frac{L}{2j}\sqrt{\frac{\gamma+\mu}{2}}\right\}. \quad (67)$$

Introducing Eq. (67) into Eq. (66), we obtain that the characteristic exponent Λ satisfies an inequality

$$\Lambda \leqslant 192\exp\left\{-\frac{L}{j}\sqrt{\frac{\gamma+\mu}{2}}\right\}. \quad (68)$$

Assuming $L=50$, $j=1$, $\gamma+\mu\sim 1$, from Eq. (68) we obtain $\Lambda<10^{-13}$. The edge state $(\tilde{\phi}_0^{(2)},0)^T$ is a neutral (Goldstone) mode ($\Lambda=0$) of Eq. (58). It follows from the translational symmetry of the problem. The excitation of this mode results in the motion of the Ising state along the system. The edge state $(\phi_0^{(2)},0)^T$ exists only in finite size systems. As it will be shown below the excitation of this mode results in the formation of a spatially uniform state. Note that when $L\to\infty$ the width of the instability interval (66) decreases, the eigenvalues which correspond to the edge states ϕ_0 and $\tilde{\phi}_0$ merge and the edge states transform into the state $\mathrm{sech}^2\,\xi$ with a double zero eigenvalue.

As it is seen from Eqs. (59) and (60) the eigenvalue problem given by Eqs. (58) also possesses eigenvectors

$$\vec{Q}_k = (0, \phi^{(1)}_{0,k}(z))^T \tag{69}$$

with eigenvalues Λ belonging to the interval

$$\frac{m}{\gamma+\mu}(\gamma-\gamma_c) \leqslant \Lambda \leqslant \frac{\gamma-\gamma_d}{\gamma+\mu}, \tag{70}$$

where the notations $\gamma_d=(1+2m)\mu$, $\gamma_c=(2+m)\mu/m$ are used. It follows from Eq. (70) that for $\gamma<\gamma_d$ all eigenvalues are negative and the Ising state is stable with respect to the excitation of the states $\phi^{(1)}_{0,k}(z)$. When $\gamma_d<\gamma<\gamma_c$ the states with small k have positive characteristic exponents Λ and they are growing in time, while for the states with k close to the upper edge of the Brillouin zone $k \leqslant \pi/2\mathbf{K}$ the characteristic exponents are negative ($\Lambda<0$). Thus for these γ the Ising state is unstable with respect to the excitation of the states $\phi^{(1)}_{0,k}(z)$ with small wave number (dn-like) and a transition to the in-phases Bloch state (43) takes place. When $\gamma>\gamma_c$ all states (69) have positive characteristic exponents. In this case the Ising-Bloch transition leads to an appearance of either the in-phase state (43) with the mean chirality $\bar{\chi}=0$ or the staggered state (45) with the mean chirality $\bar{\chi}\neq 0$. To establish the relative stability of these states one should go beyond the linear stability analysis which will be presented below.

III. NUMERICAL STUDIES

To check our results we have performed several numerical studies. To this end we carried out the dynamical simulations of the equations

$$\tau_a \partial_t X_n = J(X_{n+1} + X_{n-1} - 2X_n) + (\gamma+\mu)X_n - (X_n^2 + Y_n^2)X_n,$$

$$\tau_a \partial_t Y_n = J(Y_{n+1} + Y_{n-1} - 2Y_n) + (\gamma-\mu)Y_n - (X_n^2 + Y_n^2)Y_n \tag{71}$$

under the boundary conditions (33). These are Eqs. (35) and (36) which are written for the spatially uniform along z case.

First we checked the stability of periodic Ising states (41) for systems of different size L. This was studied by solving Eqs. (71) with the initial condition

$$X_n(0) = X_I(s) + \epsilon\phi^{(2)}_0|_{s=n}, \quad Y_n(0) = 0,$$

where $X_I(s)$ is the periodic Ising state (41) and $\phi^{(2)}_0$ is the edge state (64) with respect to which the continuum theory predicts instability of the Ising state (41). The dynamics of the Ising state for the set of parameters

$$\tau_a = 1, \quad J = 1, \quad \gamma = 1, \quad \mu = 0.05, \quad j = 1, \quad \epsilon = 10^{-3},$$

and for two different sizes of the system $L=12$ and $L=24$ is shown in Fig. 6. As it is seen from this figure in full agreement with the results obtained in the previous section the Ising state is unstable in small systems (for $L=12$ it transforms to the spatially uniform state when $t>300$), but it is a very long-lived state when the size of the system is doubled: in systems with $L=24$, even for $t\sim 10^5$ the Ising state essentially preserves its shape.

Considering the solutions to Eqs. (71) for the gain rate γ in the interval $\gamma>\gamma_c$ where in accordance with the linear stability analysis two types of the Bloch states coexist, we found that for the same set of parameters the system evolves either to a nonstaggered Bloch state or to a staggered one depending on whether nonstaggered or staggered is the initial condition. A typical time evolution for $\gamma>\gamma_c$ is shown in Figs. 7–9. Here we used the set of parameters

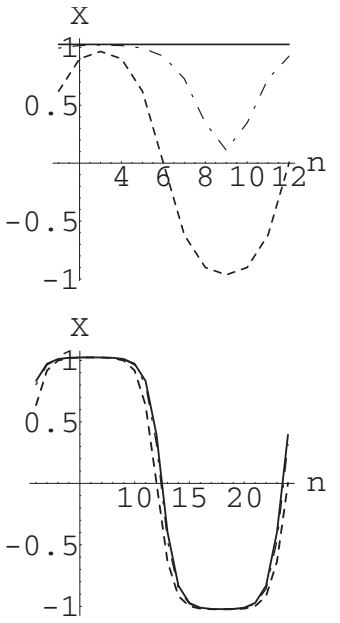

FIG. 6. The top panel shows the time evolution of the Ising state for the system with the number of sites $L=12$ for the time moments $t=0$ (dashed line), $t=270$ (dotted-dashed line), $t=300$ (solid line); the bottom shows the evolution for $L=24$ for the time moments $t=0$ (dashed line), $t=2000$ (dotted-dashed line), $t=50\,000$ (solid line).

$$\tau_a = 1, \quad J = 1, \quad \gamma = 1, \quad \mu = 0.15, \quad L = 60, \tag{72}$$

and two different types of initial conditions,

$$X_n(0) = 10^{-3}\cos\frac{2\pi}{L}n,$$

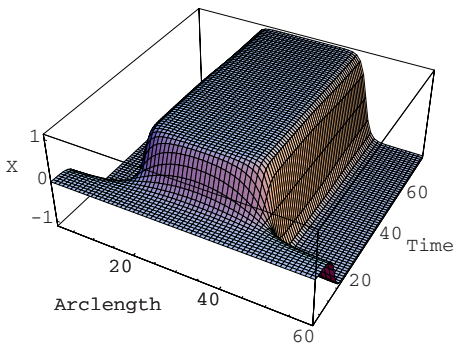

FIG. 7. (Color online) The evolution of the real part of the complex amplitude when the initial seed is given by Eq. (74).

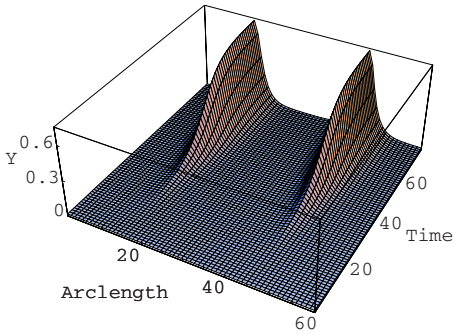

FIG. 8. (Color online) The evolution of the imaginary part of the complex amplitude when the initial seed is given by Eq. (73).

$$Y_n(0) = 10^{-3}\left(1 - 0.1\cos^2\frac{2\pi}{L}n\right), \tag{73}$$

and

$$X_n(0) = 10^{-3}\cos\frac{2\pi}{L}n,$$

$$Y_n(0) = 10^{-3}\sin\frac{2\pi}{L}n. \tag{74}$$

The final shape of the X component of the field is almost the same for both types of the initial conditions (73) and (74). In contrast to that the Y components are qualitatively different: for the initial condition (73) the system evolves to a nonstaggered Bloch state (see Fig. 8) while for Eq. (74) it evolves to a staggered Bloch state (see Fig. 9).

For large systems the interval (γ_d, γ_c) where only nonstaggered Bloch states may exist is very narrow (for $L=60$ it is $\sim 10^{-7}$), but for small and medium sized systems it may be sizable. We considered the time evolution of the system with $L=20$ and $\mu=0.15$ when $\gamma_d=0.43$, $\gamma_c=0.47$ and found out that in full agreement with the results of linear analysis for $\gamma \in (\gamma_d, \gamma_c)$ only the nonstaggered Bloch states are stable.

IV. WEAKLY NONLINEAR DYNAMICS OF BLOCH STATES

The aim of this section is to develop a weakly nonlinear approach to the dynamics of the Bloch states. We will assume that we are close to the Ising-Bloch transition and both types of the Bloch states (45) and (43) may coexist.

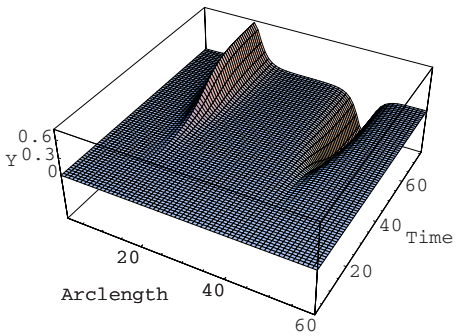

FIG. 9. (Color online) The evolution of the imaginary part of the complex amplitude when the initial seed is given by Eq. (74).

We will search for solutions of Eqs. (53) of the form

$$\vec{q} = \vec{q}_1 + \vec{q}_2 + \vec{q}_3 + \cdots, \tag{75}$$

where $\vec{q}_j=(u_j,v_j)^T \sim \epsilon^j$ (ϵ is a small parameter). The first term $\vec{q}_1=(0,v_1)^T$ is a linear superposition of the critical modes $\phi^{(1)}_{0,k}$. It is given by the expression

$$v_1 = \int A_k \phi^{(1)}_{0,k} dk, \tag{76}$$

where A_k is the amplitudes of critical modes. Taking into account that the density of critical modes diverges at the edges of the band of critical modes (see Appendix B), for large systems ($L \gg 1$), one can approximate the term $\vec{q}_1$ in Eq. (76) as a linear combination of two edge states

$$v_1 = A\ \mathrm{cn}(\xi) + B\ \mathrm{dn}(\xi), \tag{77}$$

where $A=A(\epsilon\zeta, \epsilon^2\tau)$ and $B=B(\epsilon\zeta, \epsilon^2\tau)$ are slowly varying amplitudes of critical modes.

We assume that (i) supercriticality is small,

$$|\gamma - \gamma_c|, \quad |\gamma - \gamma_d| = \mathcal{O}(\epsilon^2)$$

and (ii) the size of the system is big, $L \gg 1$, such that

$$\gamma_c - \gamma_d = 2\mu\frac{1-m^2}{m} = \mathcal{O}(\epsilon^2).$$

Inserting the expansions (75) and (77) into Eq. (53) and using a standard technique of weakly nonlinear analysis (see Appendix B for details) we obtain a system of equations for the amplitudes A and B:

$$\partial_\tau A = \partial^2_\zeta A + \Delta_c A - A^3 - 3AB^2,$$

$$\partial_\tau B = \partial^2_\zeta B + \Delta_d B - B^3 - 3A^2 B. \tag{78}$$

Thus in a weakly nonlinear approximation the dynamics of the Ginzburg-Landau model on a cylinder given by Eq. (38) reduces to the dynamics of a driven one-dimensional Ginzburg-Landau equation for the complex amplitude $\varphi=A+iB$,

$$\partial_\tau \varphi = -\frac{\delta \mathcal{F}_r}{\delta \varphi^*} \tag{79}$$

with the energy functional

$$\mathcal{F}_r = \int_{-\infty}^{\infty} d\zeta \left\{ |\partial_\zeta \varphi|^2 - \frac{1}{2}(\Delta_c + \Delta_d)|\varphi|^2 + \frac{3}{4}|\varphi|^4 - \frac{1}{2}(\Delta_c - \Delta_d)\mathrm{Re}(\varphi^2) - \frac{1}{8}\mathrm{Re}(\varphi^4) \right\}, \tag{80}$$

which is a special case of the free energy functional with biquadratic coupling between two order parameters considered a long time ago in [50]. In the reduced form the system acquires an additional nonlinear parametric driving [the last term in Eq. (80)]. This driving is a result of the existence of two types of Bloch states in the Ginzburg-Landau model on a cylinder.

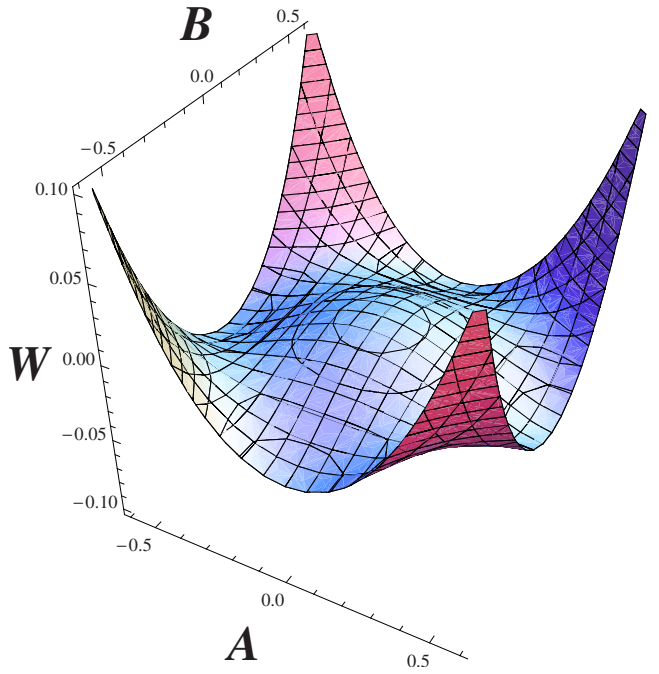

FIG. 10. (Color online) Effective energy profile for the amplitudes of staggered and unstaggered critical modes.

V. SWITCHING OF BLOCH STATE CHIRALITY BY AN EXTERNAL ac FIELD

Assuming that $\partial_\xi A=\partial_\xi B=0$, we see from Eqs. (78) that the dynamics of spatially uniform along the cylindrical z-axis states is equivalent to the overdamped dynamics of a particle moving in the two-dimensional potential

$$W=-\frac{1}{2}\Delta_c A^2-\frac{1}{2}\Delta_d B^2+\frac{1}{4}(A^4+B^4+6A^2B^2). \quad (81)$$

When $\gamma>\gamma_c$ the bifurcation parameters Δ_c and Δ_d are positive. In this case the effective potential has four wells. Two of them are situated at the points $A=\pm\sqrt{\Delta_c}$, $B=0$ and have the energy $W_A=-\Delta_c^2/4$, two others are at the points $A=0$, $B=\pm\sqrt{\Delta_d}$ and have the energy $W_B=-\Delta_d^2/4$ (see Fig. 10). Two signs of the amplitude B correspond to two different polarizations of the unstaggered Bloch state.

The shape of the effective potential (81) suggests we study a possibility to control the chirality of the periodic Bloch states by using an external driving. We investigated this possibility by augmenting the free energy functional (36) with the term

$$W_{dr}=\frac{1}{2}\sum_n (f_n e^{-i\omega t}\psi_n+\text{c.c.})$$
$$\equiv\sum_n \{f_n\cos(\omega t)X_n+f_n\sin(\omega t)Y_n\}, \quad (82)$$

where f_n is the amplitude (in general, spatially inhomogeneous) of the driving force and ω is its frequency. In the presence of the interaction (82) the equations for the critical amplitudes take the form

$$\partial_\tau A=\Delta_c A-A^3-3AB^2+f_A\sin(\bar{\omega}\tau), \quad (83)$$

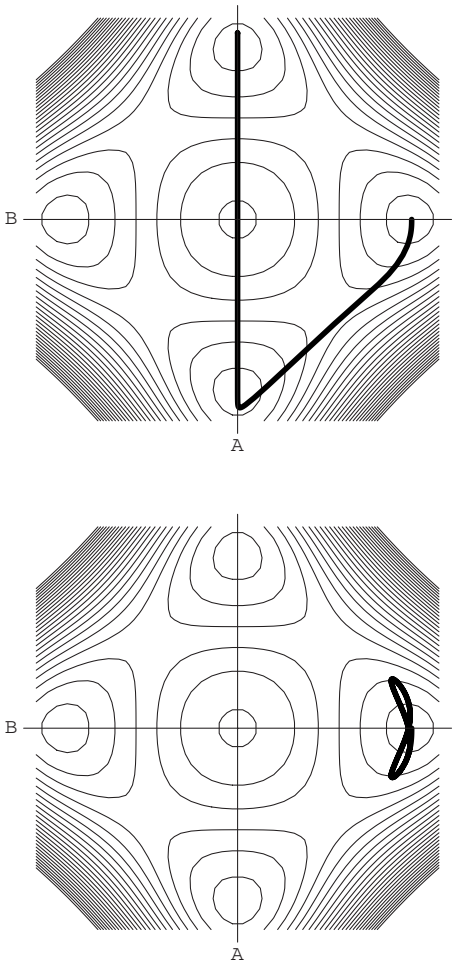

FIG. 11. Phase portrait for a switching dynamics under the action of spatially homogeneous ac field for $\gamma=1$, $\mu=0.15$, $f_B=0.1$, and two different values of the driving frequency $\omega=0.1$ (top panel), $\omega=0.25$. Initially the system is in the in-phase Bloch state.

$$\partial_\tau B=\Delta_d B-B^3-3A^2B+f_B\sin(\bar{\omega}\tau), \quad (84)$$

where $\bar{\omega}=\omega\frac{1+\mu}{\gamma+m}$ is a rescaled driving frequency and the notations

$$f_A=\frac{1}{4}\int_0^{4\mathbf{K}} f(\xi)\text{cn}(\xi)d\xi,$$

$$f_B=\frac{1}{4}\int_0^{4\mathbf{K}} f(\xi)\text{dn}(\xi)d\xi \quad (85)$$

for effective amplitudes of the driving field are used.

In the case of a spatially homogeneous external field the effective amplitude $f_A\equiv 0$ and the driving force enters Eq. (84) only. Assuming that initially the system is in the staggered Bloch state, $A(0)\neq 0$, $B(0)=0$, we obtain that if the frequency of the field $\bar{\omega}$ is below some critical value there is a switching to the in-phase Bloch state, while for high enough frequencies the system stays in the staggered state (see Fig. 11). When the system initially is in the in-phase Bloch state the chirality switching does not occur when a spatially homogeneous field is applied (see Fig. 12). How-

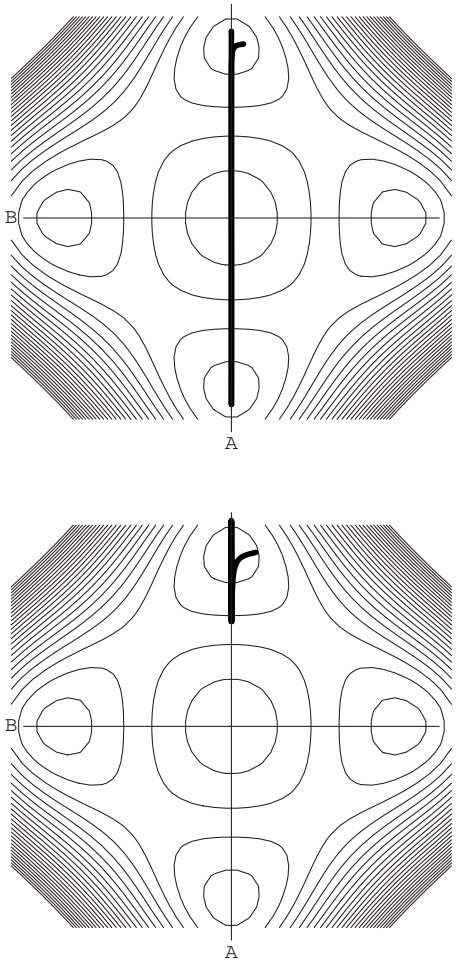

FIG. 12. Phase portrait for a switching dynamics under the action of spatially homogeneous ac field for $\gamma=1$, $\mu=0.15$, $f_B=0.1$, and two different values of the driving frequency $\omega=0.1$ (top panel), $\omega=0.25$. Initially the system is in the staggered Bloch state.

ever, under the action of cosine-like external field when the effective amplitude $f_A \neq 0$, a switching from the in-phase Bloch state to the staggered one takes place.

To verify these analytical predictions we solved numerically the equations

$$\tau_a \partial_t X_n = J(X_{n+1} + X_{n-1} - 2X_n) + (\gamma + \mu)X_n - (X_n^2 + Y_n^2)X_n + f_n \cos(\omega t),$$

$$\tau_a \partial_t Y_n = J(Y_{n+1} + Y_{n-1} - 2Y_n) + (\gamma - \mu)Y_n - (X_n^2 + Y_n^2)Y_n + f_n \sin(\omega t), \quad (86)$$

which are discrete parametrically and directly driven Ginzburg-Landau equations. We used the set of parameters (72) and by using the initial conditions (74) we first allowed the system to evolve to its stationary states without driving ($f_n=0$) and then we switched to the direct external driving. The results of the simulations are shown in Figs. 13 and 14, which were obtained for

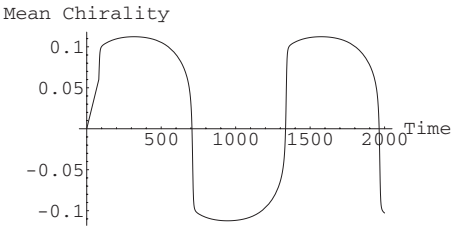

FIG. 13. Mean chirality switching from the in-phase Bloch state to the staggered Bloch state under the action of the external driving with the amplitude $f=0.1$ and the frequency $\omega=0.005$.

$$f_n = 0.1 \sin\left(\frac{2\pi}{L} n\right), \quad \omega = 0.005.$$

In the same way by applying a spatially homogeneous external driving with the same amplitude and frequency one can achieve a switching from the staggered Bloch state to the in-phase one.

VI. CONCLUSIONS

In this paper, we have discussed the dynamics of nonlinear excitations in two-dimensional parametrically driven Ginzburg-Landau equation models with nonlinearity management. We have considered a system of alternating active and passive waveguides placed along a circumference. We have derived a set of pseudodifferential equations, i.e., nonlocal in space and time equations, which govern the nonlinear dynamics in active waveguides. We have shown that the nonlocality of the problem is of prime importance in the systems where the excitations in passive regions are undamped and have a large coherence length. We found that in addition to a usual Ising-Bloch instability the Ising domain walls in systems with long-range dispersion experience instability with respect to softening of a shape mode. In this paper we have been mainly concerned with the case when the damping in the idle regions is large. In this case the dynamics is described by a set of L linearly coupled one-dimensional Ginzburg-Landau equations. We investigated the stationary solutions of this set of equations and their stability. We have found that there are three kinds of station-

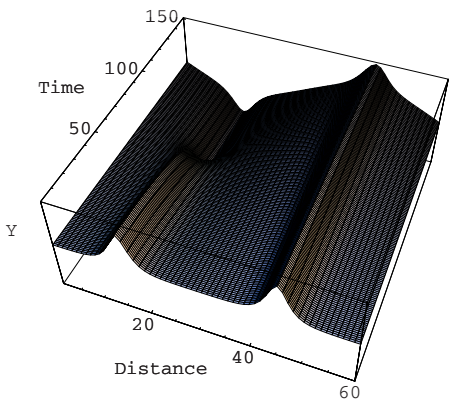

FIG. 14. (Color online) The Bloch state evolution for the same parameters as in Fig. 13.

ary solutions. For the solutions of the first kind only one component (real or imaginary) of the complex amplitude in the active region is active. These are periodic Ising states. In addition to them there exist *two kinds* of periodic solutions in which both components of the complex amplitude are active: staggered and unstaggered Bloch states. These two Bloch states are characterized by different chirality density profiles: the staggered states are characterized by a finite mean chirality, while in the unstaggered ones the mean chirality is zero.

The linear stability analysis showed that the Ising periodic states are, strictly speaking, unstable. However, this instability is important only for systems with few active waveguides. For a large number of active waveguides L their lifetime is exponentially big. When the gain rate in the active regions is high the two types of the Bloch states coexist. The weakly nonlinear analysis showed that the nonlinear dynamics of the Bloch states is described by a complex Ginzburg-Landau equation with linear and nonlinear parametric driving. It is shown that under the action of ac external field one can switch between the staggered and unstaggered Bloch states.

ACKNOWLEDGMENTS

The authors thank Preben Buchhave for illuminating discussions. Yu.B.G. acknowledges funding by Otto Mønsteds Fond. He also acknowledges support from Civilingeniør Frederik Christiansens ALMENNYTTIGE FOND and MIDIT, FNU Grant No. 21-02-0500. He acknowledges the Department of Physics, Technical University of Denmark for its hospitality.

APPENDIX A

In this appendix we derive the set of equations (4)–(6). We will follow the procedure which previously was developed for nonlinear Schrödinger-Kronig-Penney models [21] and for a superlattice of Josephson junctions [54]. Using the Fourier transform with respect to z and the Laplace transform with respect to t (denoted by the overbar)

$$\bar{\psi}(s,k,\omega)=\frac{1}{(2\pi)}\int_{-\infty}^{\infty}dz\int_{0}^{\infty}dt\psi(s,z,t)e^{-ikz-\omega t}, \quad \text{(A1)}$$

one can represent Eq. (2) in the idle regions

$$\lambda n+\frac{w}{2}<s<\lambda(n+1)-\frac{w}{2}, \quad n=0,\pm 1,\pm 2,\ldots, \quad \text{(A2)}$$

in the form

$$(\ell_{id}^2k^2+\omega\tau_i+\gamma_i)\bar{\psi}(s,k,\omega)-\ell^2\partial_s^2\bar{\psi}(s,k,\omega)=0. \quad \text{(A3)}$$

In the windows

$$|s-\lambda n|<\frac{w}{2}, \quad n=0,\pm 1,\pm 2,\ldots, \quad \text{(A4)}$$

the corresponding equation is

$$(\ell_a^2k^2+\omega\tau_a)\bar{\psi}(s,k,\omega)=\ell^2\partial_s^2\bar{\psi}(s,k,\omega)+\overline{F(\psi,\psi^*)}. \quad \text{(A5)}$$

The solution of Eq. (A3) in the interval (A2) has the form

$$\bar{\psi}(s,k,\omega)=A_n(k,\omega)e^{-\kappa s/\ell}+B_n(k,\omega)e^{\kappa s/\ell}, \quad \text{(A6)}$$

where

$$\kappa=\sqrt{\ell_{id}^2k^2+\omega\tau_i+\gamma_i}. \quad \text{(A7)}$$

The condition that the phase ψ and its derivative $\partial_s\psi$ be continuous at the interfaces between windows and idle regions leads to the relations

$$A_ne^{-\kappa[\lambda n+(w/2)]/\ell}+B_ne^{\kappa[\lambda n+(w/2)]/\ell}=\bar{\psi}_w\left(\lambda n+\frac{w}{2},k,\omega\right), \quad \text{(A8a)}$$

$$A_ne^{-\kappa[\lambda n+(w/2)]/\ell}-B_ne^{\kappa[\lambda n+(w/2)]/\ell}=-\frac{L}{\kappa}\partial_s\bar{\psi}_w\,(s,k,\omega)|_{s=\lambda n+(w/2)}, \quad \text{(A8b)}$$

where $\bar{\psi}_w(s,k,\omega)$ is the solution of the window equation (A5). Let us integrate Eq. (A5) with respect to s over the n_{th} window. As a result we obtain

$$\partial_s\bar{\psi}_w\,(s,k,\omega)|_{s=\lambda n+(w/2)}-\partial_s\bar{\psi}_w\,(s,k,\omega)|_{s=\lambda n-(w/2)}=\frac{\kappa_a^2}{\ell^2}\int_{\lambda n-w/2}^{\lambda n+(w/2)}ds\bar{\psi}_w(k,\omega)-\frac{1}{\ell^2}\int_{\lambda n-(w/2)}^{\lambda n+(w/2)}ds\overline{F(\psi,\psi^*)}=0, \quad \text{(A9)}$$

where

$$\kappa_a^2=\ell_a^2k^2+\omega\tau_a+\gamma_i. \quad \text{(A10)}$$

Taking into account the boundary conditions given by Eqs. (A8a) and (A8b) we can represent Eq. (A9) in the form

$$\frac{\ell\kappa}{\sinh(\kappa d)}\left[\bar{\psi}_w\left((n+1)\lambda-\frac{w}{2},k,\omega\right)+\bar{\psi}_w\left((n-1)\lambda+\frac{w}{2},k,\omega\right)\right]-\frac{\ell\kappa}{\tanh(\kappa d)}\left[\bar{\psi}_w\left(n\lambda+\frac{w}{2},k,\omega\right)+\bar{\psi}_w\left(n\lambda-\frac{w}{2},k,\omega\right)\right]=\kappa_a^2\int_{\lambda n-(w/2)}^{\lambda n+(w/2)}ds\bar{\psi}_w(s,k,\omega)-\int_{\lambda n-(w/2)}^{\lambda n+(w/2)}ds\overline{F(\psi,\psi^*)}, \quad \text{(A11)}$$

where $d=(\lambda-w)/\ell$ is the width of the idle region measured in terms of the coherence length ℓ. In the limit of thin windows one can neglect the variation of the window function across the window,

$$\bar{\psi}_w(s,k,\omega)\equiv\bar{\psi}_n(k,\omega), \quad s\in\left(n\lambda-\frac{w}{2},n\lambda+\frac{w}{2}\right),$$

$$n=0,\pm 1,\pm 2,\ldots \quad \text{(A12)}$$

and obtain that the dynamics of the system is governed by the set of equations

$$\frac{\ell\kappa}{\sinh(\kappa d)}[\bar{\psi}_{n+1}(k,\omega)+\bar{\psi}_{n-1}(k,\omega)]-\frac{2\ell\kappa}{\tanh(\kappa d)}\bar{\psi}_n(k,\omega)$$
$$=\ell_a^2 w\bar{\psi}_n(k,\omega)-w\overline{F(\psi,\psi^*)}_n(k,\omega), \tag{A13}$$

where $n=0,\pm1,\pm2,\ldots$. Using the inverse Fourier and Laplace transforms we can represent Eqs. (A13) in real space and time variables as follows:

$$\tau_a\partial_t\psi_n(z,t)=\ell_a^2\partial_z^2\psi_n(z,t)+\gamma_a\psi_n(z,t)+\mu\psi_n^*(z,t)$$
$$-|\psi_n(z,t)|^2\psi_n(z,t)+\frac{\ell\hat{\kappa}}{w\sinh(\hat{\kappa}d)}[\psi_{n+1}(z,t)$$
$$+\psi_{n-1}(z,t)]-\frac{2\ell\hat{\kappa}}{w\tanh(\hat{\kappa}d)}\psi_n(z,t),$$
$$n=0,\pm1,\pm2,\ldots, \tag{A14}$$

where $\hat{\kappa}\equiv\sqrt{-\ell_{id}^2\partial_z^2+\tau_i\partial_t+\gamma_i}$ is the pseudodifferential operator defined as

$$\overline{\hat{\kappa}\psi}(k,\omega)\equiv\frac{1}{2\pi}\int_{-\infty}^{\infty}dz\int_0^{\infty}dte^{-ikz-\omega t}\sqrt{-\ell_{id}^2\partial_z^2+\tau_i\partial_t+\gamma_i}\psi(z,t)$$
$$=\sqrt{\ell_{id}^2k^2+\tau_i\omega+\gamma_i}\bar{\psi}(k,\omega). \tag{A15}$$

When the complex amplitudes are the same in all active waveguides,

$$\psi_n(z,t)=\Psi(z,t), \tag{A16}$$

the complex amplitude $\Psi(z,t)$ satisfies the equation

$$\tau_a\partial_t\Psi(z,t)=\ell_a^2\partial_z^2\Psi(z,t)+\gamma_a\Psi(z,t)+\mu\Psi^*(z,t)$$
$$-|\Psi(z,t)|^2\Psi(z,t)-\frac{2\ell}{w}\hat{\kappa}\tanh(\hat{\kappa}d/2)\Psi(z,t). \tag{A17}$$

The nonlocal character of the active area dynamics is clearly seen if we consider the last term on the right-hand side of Eq. (A17). Taking into account the well-known expansion in a series of simple fractions [55] and the definition (A15) of the operator $\hat{\kappa}$, we can write

$$\hat{\kappa}\tanh(\hat{\kappa}d)\Psi(z,t)=4d\sum_{n=1}^{\infty}\frac{\hat{\kappa}^2}{\hat{\kappa}^2d^2+(2n-1)^2\pi^2}\Psi(z,t)$$
$$=\int_{-\infty}^{\infty}dz'\int_0^t dt'\mathcal{K}(z-z',t-t')(-\ell_{id}^2\partial_{z'}^2$$
$$+\tau_i\partial_{t'}+\gamma_i)\Psi(z',t'), \tag{A18}$$

where the kernel $\mathcal{K}(z-z',t-t')$ is given by the expression

$$\mathcal{K}(z,t)=\frac{2}{\tau_i d}\sqrt{\frac{\pi}{D_{id}t}}\theta_2(0,e^{-4\pi^2t/d^2\tau_i})\exp\left\{-\frac{z^2}{4D_{id}t}-\gamma_i\frac{t}{\tau_i}\right\}, \tag{A19}$$

where $D_{id}=\ell_{id}^2/\tau_i$ is the diffusion coefficient in the idle region, and $\theta_2(x,q)$ is the Jacobi theta function [55]. The nonlocal effects or, in other words, effects of long-range coupling and long memory effects, are particularly well pronounced in systems where in the idle region excitations have a big diffusion coefficient D_{id} and a long lifetime τ_i/γ_i. In the limit $\tau_i\to0$ the memory effects in the idle region may be neglected and

$$\mathcal{K}(z-z',t-t')=2\delta(t-t')\mathcal{G}(z-z') \tag{A20}$$

with the kernel $\mathcal{G}(z-z')$ being determined by the expression

$$\mathcal{G}(z-z')=\frac{4\pi}{\ell_{id}}\sum_{n=1}^{\infty}\frac{\exp[-\sqrt{\gamma_i+(2n-1)^2/d^2}|z-z'|/\ell_{id}]}{\sqrt{\gamma_i+(2n-1)^2/d^2}}$$
$$\approx\frac{4\pi}{\ell_{id}}\frac{\exp(-\sqrt{\gamma_i+1/d^2}|z-z'|/\ell_{id})}{\sqrt{\gamma_i+1/d^2}}. \tag{A21}$$

When the distance between active waveguides increases the interwaveguide coupling [the last term in the right-hand side of Eqs. (4)] vanishes and the equation takes the form

$$\tau_a\partial_t\Psi(z,t)=\ell_a^2\partial_z^2\Psi(z,t)+\gamma_a\Psi(z,t)+\mu\Psi^*(z,t)$$
$$-|\Psi(z,t)|^2\Psi(z,t)-\frac{2\ell}{w}\sqrt{-\ell_{id}^2\partial_z^2+\tau_i\partial_t+\gamma_i}\Psi(z,t). \tag{A22}$$

If the lifetime of excitations in the idle region is infinitely long ($\gamma_i\to0$), Eq. (A22) reduces to the equation

$$\tau_a\partial_t\Psi(z,t)=\ell_a^2\partial_z^2\Psi(z,t)+\gamma_a\Psi(z,t)+\mu\Psi^*(z,t)$$
$$-|\Psi(z,t)|^2\Psi(z,t)-\frac{2\ell}{w}\sqrt{-\ell_{id}^2\partial_z^2+\tau_i\partial_t}\Psi(z,t), \tag{A23}$$

which belongs to the category of fractional GL equations [56,57]. In the limit $\tau_i\to0$ the last term in the right-hand side of Eq. (A23) can be expressed as a Hilbert transform of the function $\partial_z\Psi$ [58], and by analogy with the case of the nonlinear Hilbert-Schrödinger equation introduced in Refs. [21,59] may be called the Hilbert-Ginzburg-Landau equation.

APPENDIX B

The aim of this appendix is to develop a weakly nonlinear approach to the dynamics of the Bloch states. We will assume that we are close to the Ising-Bloch transition and both types of the Bloch states (43) and (45) may coexist.

We will search for solutions of Eqs. (53) of the form

$$\vec{q}=\vec{q}_1+\vec{q}_2+\vec{q}_3+\cdots, \tag{B1}$$

where $\vec{q}_j\sim\epsilon^j$ (ϵ is a small parameter). The first term $\vec{q}_1=(0,v_1)^T$ is a linear superposition of the critical modes $\phi_{0,k}^{(1)}$. It is given by the expression

$$v_1=\int A_k\phi_{0,k}^{(1)}dk, \tag{B2}$$

where A_k is the amplitudes of critical modes.

We are now going to show that in large enough systems the most important critical modes which govern the Ising-

Bloch transition in periodic systems are the edge modes. The vector $\vec{q}_1$ from Eq. (B2) can be presented in the form

$$v_1 = \int A_k \phi^{(1)}_{0,k} dk = \int_{E_0}^{\tilde{E}_0} \rho(\mathcal{E}) f(\mathcal{E}) d\mathcal{E}, \tag{B3}$$

where

$$\rho(\mathcal{E}) = \frac{dk}{d\mathcal{E}} \tag{B4}$$

is the density of the critical modes. The function $k(\mathcal{E})$ gives the dispersion of critical modes, $E_0=m$ and $\tilde{E}_0=1$ are the edges of the band, and the abbreviation

$$f(\mathcal{E}) = A_{k(\mathcal{E})} \phi^{(1)}_{0,k(\mathcal{E})} \tag{B5}$$

is used. Using the dispersion relation for the lowest band of the Lamé equation (55) with $l=1$ which was obtained in [53], one can obtain that the density of critical modes is given by the expression

$$\rho(\mathcal{E}) = \frac{\mathbf{E} - (\mathcal{E} - E_0)\mathbf{K}}{2\mathbf{K}\sqrt{(\tilde{E}_0 - \mathcal{E})(\mathcal{E} - E_0)(E_1 - \mathcal{E})}} \quad \text{for } \mathcal{E} \in (E_0, \tilde{E}_0), \tag{B6}$$

where $E_1=1+m$. Thus, the density of states is singular at the band edges E_0 and $\tilde{E}_0$. In large enough systems ($L \gg 1$) the bandwidth of the critical modes is small: $\tilde{E}_0 - E_0 = 1 - m \ll 1$. Assuming that the function $f(\mathcal{E})$ is smooth, for $\mathcal{E} \in (E_0, \tilde{E}_0)$ one can approximate it as follows:

$$f(\mathcal{E}) \approx f(E_0) + \frac{\mathcal{E} - E_0}{\tilde{E}_0 - E_0}[f(\tilde{E}_0) - f(E_0)]. \tag{B7}$$

Inserting Eqs. (B6) and (B7) into Eq. (B3), after small calculations we obtain

$$v_1 = \frac{\pi}{2\mathbf{K}} f(E_0) + \frac{1}{1-m}\left(\frac{\mathbf{E}}{\mathbf{K}}(\mathbf{K}' - \mathbf{E}') - \frac{3-m}{3}\mathbf{K}' + 2\frac{(2-m)}{3}\mathbf{E}'\right)[f(\tilde{E}_0) - f(E_0)], \tag{B8}$$

where $\mathbf{E}'=\mathbf{E}(1-m)$, $\mathbf{K}'=\mathbf{K}(1-m)$. For $L \gg 1$, when $m \approx 1$ it reduces to

$$v_1 = \frac{\pi}{4\mathbf{K}}[f(E_0) + f(\tilde{E}_0)]. \tag{B9}$$

Recalling the definition (B5), one can conclude that in large systems the main contribution to the first-order vector $\vec{q}_1$ is due to the edge states and this vector can be presented as follows:

$$v_1 = A\ \mathrm{cn}(\xi) + B\ \mathrm{dn}(\xi), \tag{B10}$$

where $A=A(\epsilon\zeta, \epsilon^2\tau)$ and $B=B(\epsilon\zeta, \epsilon^2\tau)$ are slowly varying edge amplitudes (order parameters).

We assume that (i) supercriticality is small,

$$|\gamma - \gamma_c|, \quad |\gamma - \gamma_d| = \mathcal{O}(\epsilon^2),$$

and (ii) the size of the system is big, $L \gg 1$, such that

$$\gamma_c - \gamma_d = 2\mu\frac{1-m^2}{m} = \mathcal{O}(\epsilon^2).$$

Inserting the expansions (B1) and (B10) into Eq. (53) we obtain

$$\epsilon^1: \quad \hat{\mathcal{H}}_0 \vec{q}_1 = 0, \tag{B11}$$

where $\hat{\mathcal{H}}_0 \equiv \hat{\mathcal{H}}|_{\gamma=\gamma_d}$,

$$\epsilon^2: \quad (\hat{H}_2 - 1 - m)u_2 = 2mv_1^2\ \mathrm{sn}(\xi), \tag{B12}$$

$$\epsilon^3: \quad (-\hat{H}_2 + 1 + m)u_2 = 0, \tag{B13}$$

$$(-\hat{H}_1 + m)v_3 = \partial_\tau v_1 - A\Delta_c\ \mathrm{cn}(\xi) - B\Delta_d\ \mathrm{dn}(\xi) + 4mv_1u_2\ \mathrm{sn}(\xi) + 2mv_1^3, \tag{B14}$$

where the operator H_l is given by Eq. (55) and the notations

$$\Delta_c = m\frac{\gamma - \gamma_c}{\gamma + \mu}, \qquad \Delta_d = \frac{\gamma - \gamma_d}{\gamma + \mu} \tag{B15}$$

are used. Taking into account that the homogeneous equation $(\hat{H}_2 - 1 - m)\ g=0$ has two linearly independent solutions of the form

$$g_1 = \mathrm{cn}(\xi)\mathrm{dn}(\xi),$$

$$g_2 = \left[\left(1 - m - (1+m)\frac{\mathbf{E}}{\mathbf{K}}\right)\xi + [dc(\xi) + m^2 cd(\xi)]\mathrm{sn}(\xi) - (1+m)Z(\xi|m)\right]g_1 \tag{B16}$$

where $Z(\xi|m)$ is Jacobi's zeta function [49], it is straightforward to find that the solution of the second-order equation (B12) is given by

$$u_2(\xi) = \frac{2m}{(1-m)^2}\int_0^\xi [g_1(\xi')g_2(\xi) - g_1(\xi)g_2(\xi')]v_1^2(\xi')\mathrm{sn}(\xi')d\xi'. \tag{B17}$$

The solvability conditions of the equation (B14) have the form

$$\int_0^{4\mathbf{K}} \{\partial_\tau v_1 - \partial_\xi^2 v_1 - A\Delta_c\ \mathrm{cn}(\xi) - B\Delta_d\ \mathrm{dn}(\xi) + 4mv_1u_2\ \mathrm{sn}(\xi) + 2mv_1^3\}\mathrm{dn}(\xi)d\xi = 0, \tag{B18}$$

$$\int_0^{4\mathbf{K}} \{\partial_\tau v_1 - \partial_\xi^2 v_1 - A\Delta_c \,\mathrm{cn}(\xi) - B\Delta_d \,\mathrm{dn}(\xi) + 4mv_1u_2 \,\mathrm{sn}(\xi) + 2mv_1^3\}\mathrm{cn}(\xi)d\xi = 0. \tag{B19}$$

The first condition is because the function $\mathrm{dn}(\xi)$ is a zero mode for the operator $\hat{H}_1 - m$. The second one follows from the fact that the quantity

$$\int_0^{4\mathbf{K}} \mathrm{cn}(\xi)(\hat{H}_1 - m)v_3 d\xi = (1-m)\int_0^{4\mathbf{K}} \mathrm{cn}(\xi)v_3 d\xi = \mathcal{O}(\epsilon^5) \tag{B20}$$

and hence is of higher-order smallness than the integral in the left-hand side of Eq. (B19), which is $\mathcal{O}(\epsilon^3)$. The solvability conditions (B18) and (B19) give a system of equations for the amplitudes A and B,

$$\partial_\tau A = \partial_\xi^2 A + \Delta_c A - A^3 - 3AB^2,$$

$$\partial_\tau B = \partial_\xi^2 B + \Delta_d B - B^3 - 3A^2 B. \tag{B21}$$

All other integrals which enter solvability conditions (B18) and (B19) were evaluated in the limit $m \to 1$.

[1] I. S. Aronson and L. Kramer, Rev. Mod. Phys. **74**, 99 (2002).
[2] J. W. Miles, J. Fluid Mech. **148**, 451 (1984).
[3] W. Zhang and J. Viñals, Phys. Rev. Lett. **74**, 690 (1995).
[4] B. Denardo, B. Galvin, A. Greenfield, A. Larraza, S. Putterman, and W. Wright, Phys. Rev. Lett. **68**, 1730 (1992).
[5] G. Huang, S.-Y. Lou, and M. G. Velarde, Int. J. Bifurcation Chaos Appl. Sci. Eng. **6**, 1775 (1996).
[6] K. Staliunas, J. Mod. Opt. **42**, 1261 (1995).
[7] S. Longhi, Opt. Lett. **21**, 860 (1996); J. Mod. Opt. **43**, 1089 (1996).
[8] V. J. Sánchez-Morcillo, I. Pérez-Arjona, F. Silva, G. J. Valcàrcel, and E. Roldán, Opt. Lett. **25**, 957 (2000).
[9] L. N. Bulaevski and V. L. Ginzburg, Zh. Eksp. Teor. Fiz. **45**, 772 (1963) [Sov. Phys. JETP **18**, 530 (1964)].
[10] T. Yasui, H. Tutu, M. Yamamoto, and H. Fujisaka, Phys. Rev. E **66**, 036123 (2002).
[11] I. V. Barashenkov, S. R. Woodford, and E. V. Zemlyanaya, Phys. Rev. Lett. **90**, 054103 (2003).
[12] S. Woodford and I. V. Barashenkov, J. Phys. A: Math. Theor. **41**, 185203 (2008).
[13] V. Petrov, Q. Quyang, and L. Swinney, Nature (London) **388**, 655 (1997).
[14] B. Marts, A. Hagberg, E. Meron, and A. L. Lin, Phys. Rev. Lett. **93**, 108305 (2004).
[15] B. A. Malomed, *Soliton Management in Periodic Systems* (Springer-Verlag, Berlin, 2006).
[16] *Photonic Band Gaps and Localization*, edited by C. M. Soukoulis (Plenum, New York, 1993); *Photonic Band Gap Materials*, edited by C. M. Soukoulis (Kluwer Academic Publishers, London, 1996).
[17] A. Mekis, J. C. Chen, I. Kurland, S. Fan, P. R. Villeneuve, and J. D. Joannopoulos, Phys. Rev. Lett. **77**, 3787 (1996).
[18] S. Noda, A. Alongkarn, and M. Imada, Nature (London) **407**, 608 (2000).
[19] I. Gabitov and S. Turitsyn, Opt. Lett. **21**, 327 (1996).
[20] B. Eiermann, P. Treutlein, Th. Anker, M. Albiez, M. Taglieber, K.-P. Marzlin, and M. K. Oberthaler, Phys. Rev. Lett. **91**, 060402 (2003).
[21] Yu. B. Gaididei, P. L. Christiansen, K. Ø. Rasmussen, and M. Johansson, Phys. Rev. B **55**, R13365 (1997).
[22] L. Bergé, V. K. Mezentsev, J. J. Rasmussen, P. L. Christiansen, and Yu. B. Gaididei, Opt. Lett. **25**, 1037 (2000).
[23] I. Towers and B. A. Malomed, J. Opt. Soc. Am. B **19**, 537 (2002).
[24] M. Centurion, M. A. Porter, P. G. Kevrekidis, and D. Psaltis, Phys. Rev. Lett. **97**, 033903 (2006).
[25] H. Saito and M. Ueda, Phys. Rev. Lett. **90**, 040403 (2003).
[26] F. Kh. Abdullaev, J. G. Caputo, R. A. Kraenkel, and B. A. Malomed, Phys. Rev. A **67**, 013605 (2003).
[27] K. M. Gundu, M. Kolesik, and J. V. Moloney, Opt. Lett. **32**, 763 (2007); L. Li, A. Schülzgen, H. Li, V. L. Temyanko, J. V. Moloney, and N. Peyghambarian, J. Opt. Soc. Am. B **24**, 1721 (2007).
[28] D. T. Walton and H. G. Winful, Opt. Lett. **18**, 720 (1993).
[29] B. A. Malomed and H. G. Winful, Phys. Rev. E **53**, 5365 (1996); J. Atai and B. A. Malomed, *ibid.* **54**, 4371 (1996).
[30] H. Sakaguchi, Prog. Theor. Phys. **93**, 491 (1995).
[31] E. Marti-Panameno, L. C. Gomez-Pavon, A. Luis-Ramos, M. M. Mendez-Otero, and M. D. I. Castillo, Opt. Commun. **194**, 409 (2001).
[32] A. Sigler and B. A. Malomed, Physica D **212**, 305 (2005).
[33] B. A. Malomed, Chaos **17**, 037117 (2007).
[34] A. Sigler, B. A. Malomed, and D. V. Skryabin, Phys. Rev. E **74**, 066604 (2006).
[35] P. Coullet, J. Lega, B. Houchmanzadeh, and J. Lajzerowicz, Phys. Rev. Lett. **65**, 1352 (1990).
[36] S. Sarker, S. E. Trullinger, and A. R. Bishop, Phys. Lett. **59A**, 255 (1976).
[37] D. V. Skryabin, A. Yulin, D. Michaelis, W. J. Firth, G.-L. Oppo, U. Peschel, and F. Lederer, Phys. Rev. E **64**, 056618 (2001).
[38] D. Michaelis, U. Peschel, F. Lederer, D. V. Skryabin, and W. J. Firth, Phys. Rev. E **63**, 066602 (2001).
[39] I. V. Barashenkov, S. R. Woodford, and E. V. Zemlyanaya, Phys. Rev. E **75**, 026604 (2007).
[40] I. V. Barashenkov and S. R. Woodford, Phys. Rev. E **75**, 026605 (2007).
[41] I. V. Barashenkov and S. R. Woodford, Phys. Rev. E **71**, 026613 (2005).
[42] I. V. Barashenkov, E. V. Zemlyanaya, and M. Bär, Phys. Rev.

E **64**, 016603 (2001).
[43] I. V. Barashenkov and E. V. Zemlyanaya, SIAM J. Appl. Math. **64**, 800 (2004).
[44] I. V. Barashenkov, N. V. Alexeeva, and E. V. Zemlyanaya, Phys. Rev. Lett. **89**, 104101 (2002).
[45] D. Tanaka and Y. Kuramoto, Phys. Rev. E **68**, 026219 (2003).
[46] V. García-Morales and K. Krischer, Phys. Rev. Lett. **100**, 054101 (2008).
[47] *Padé Approximants Method and its Applications to Mechanics*, edited by H. Cabanes (Springer-Verlag, Berlin, 1976).
[48] S. F. Mingaleev, Yu. B. Gaididei, E. Majerníkova, and S. Shpyrko, Phys. Rev. E **61**, 4454 (2000).
[49] M. Abramowitz and I. Stegun, *Handbook of Mathematical Functions* (Dover Publications, New York, 1972).
[50] B. Houchmandzadeh, J. Laizerowicz, and E. Salje, J. Phys.: Condens. Matter **3**, 5163 (1991).
[51] H. Bateman and A. Erdélyi, *Higher Transcendental Functions* (McGraw-Hill, New York, 1953), Vol. 3.
[52] F. Finkel, A. González-López, and M. Rodríguez, J. Phys. A **33**, 1519 (2000).
[53] Hui Li, D. Kuznetsov, and F. Iachello, J. Phys. A **33**, 6413 (2000).
[54] Y. Gaididei, N. Lazarides, and N. Flytzanis, J. Phys. A **35**, 10409 (2002).
[55] I. S. Gradstein and I. M. Ryzhik, *Handbook of Integrals, Series, and Products* (Academic Press, New York, 1965).
[56] V. E. Tarasov and G. M. Zaslavsky, Physica A **354**, 249 (2005).
[57] A. V. Milovanov and J.-J. Rasmussen, Phys. Lett. A **337**, 75 (2005).
[58] A. Erdélyi, W. Magnus, F. Oberhettinger, and F. G. Tricomi *Tables of Integral Transforms* (McGraw-Hill, New York, 1954), Vol. 2.
[59] Yu. B. Gaididei, S. F. Mingaleev, P. L. Christiansen, and K. Ø. Rasmussen, Phys. Rev. E **55**, 6141 (1997).